THE JOURNAL OF PHYSICAL CHEMISTRY C

Article

Cite This: J. Phys. Chem. C 2018, 122, 17406−17412

pubs.acs.org/JPCC

Structural Contributions to Hydrodynamic Diameter for Quantum Dots Optimized for Live-Cell Single-Molecule Tracking

Janet Y. Sheung,[†,‡,¶] Pinghua Ge,[†,¶] Sung Jun Lim,[§,∥,⊥] Sang Hak Lee,[†,¶] Andrew M. Smith,[§,∥,#] and Paul R. Selvin*[,†,¶]

[†]Department of Physics, University of Illinois at Urbana-Champaign, Champaign, Illinois 61801, United States

[‡]Department of Physics and Astronomy, Vassar College, Poughkeepsie, New York 12604, United States

[§]Department of Bioengineering, [∥]Micro and Nanotechnology Laboratory, [#]Department of Materials Science and Engineering and [¶]Center for the Physics of Living Cells, University of Illinois at Urbana−Champaign, Champaign, Illinois 61801, United States

[⊥]Intelligent Devices and Systems Research Group, DGIST, 333 Techno Jungang-Daero, Hyeonpung, Daegu 42988, Republic of Korea

Supporting Information

ABSTRACT: Quantum dots are fluorescent nanoparticles with narrow-band, size-tunable, and long-lasting emission. Typical formulations used for imaging proteins in cells are hydrodynamically much larger than the protein targets, so it is critical to assess the impact of steric effects deriving from hydrodynamic size. This report analyzes a new class of quantum dots that have been engineered for minimized size specifically for imaging receptors in narrow synaptic junctions between neurons. We use fluorescence correlation spectroscopy and transmission electron microscopy to calculate the contributions of the crystalline core, organic coating, and targeting proteins (streptavidin) to the total hydrodynamic diameter of the probe, using a wide range of core materials with emission spanning 545−705 nm. We find the contributing thickness of standard commercial amphiphilic polymers to be ∼8 to ∼14 nm, whereas coatings based on the compact ligand HS-$(CH_2)_{11}$-$(OCH_2CH_2)_4$-OH contribute ∼6 to ∼9 nm, reducing the diameter by ∼2 to ∼5 nm, depending on core size. When the number of streptavidins for protein targeting is minimized, the total diameter can be further reduced by ∼5 to ∼11 nm, yielding a diameter of 13.8−18.4 nm. These findings explain why access to the narrow synapse derive primarily from the protein functionalization of commercial variants, rather than the organic coating layers. They also explain why those quantum dots with size around 14 nm with only a few streptavidins can access narrow cellular structures for neuronal labeling, whereas those >27 nm and a large number of streptavidins, cannot.

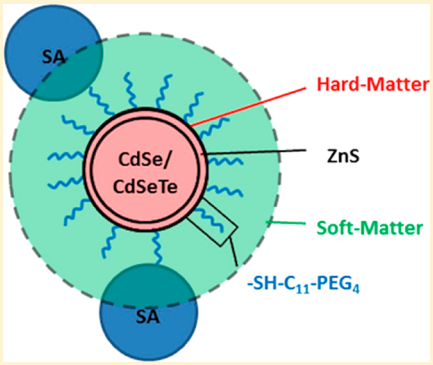

INTRODUCTION

Quantum dots (QDs) are revolutionary fluorescent probes for live-cell single-molecule imaging.[1−3] Their popularity results from their unique photophysical characteristics, including high photon emission rate for precise localization, high photostability for sustained emission over the duration of an experiment, and narrow-band emission to minimize spectral cross-talk in multicolor experiments.[4−6] Broad use has further been enabled by the commercial availability of QDs in a variety of colors and functional chemistries. Despite these advantages, the use of commercial QDs in living cells and tissues is complicated by their large hydrodynamic diameter, typically ∼15−30 nm, as well as their tendency to cross-link labeling targets due to an excess of surface functional groups.[7] This is particularly problematic when molecular targets localize to cellular regions crowded with macromolecules—which commercial QDs may be too bulky to access.[8,9] For example, when labeling a neuronal receptor within the neuronal synapse, a 20−40 nm intercellular junction filled with proteins, we observed that commercial QD labels lead to inaccurate observations that the receptors are extra-synaptic and highly mobile.[10,11] By labeling the receptors with a smaller, custom designed quantum dot, we found that receptors in the synapse were preferentially labeled and they tended to be spatially constrained.

In order to explore the underlying cause of the inconsistent observations between the different QD variants in living cells, we undertook a systematic analysis of dependence of QD hydrodynamic properties on its structure and size. The hydrodynamic size of a biofunctionalized QD arises from three constituent physical domains: (1) the crystalline fluorescent core, (2) a hydrophilic layer that renders the QD dispersible in aqueous media, and (3) biofunctional groups for specific labeling (Figure 1A).[12] The core contributes (part 1) substantially to the total size, but it can be easily engineered to the size range of 2−3 nm diameter; the coating and functional

Received: March 15, 2018
Revised: July 1, 2018
Published: July 11, 2018

DOI: 10.1021/acs.jpcc.8b02516
J. Phys. Chem. C 2018, 122, 17406−17412

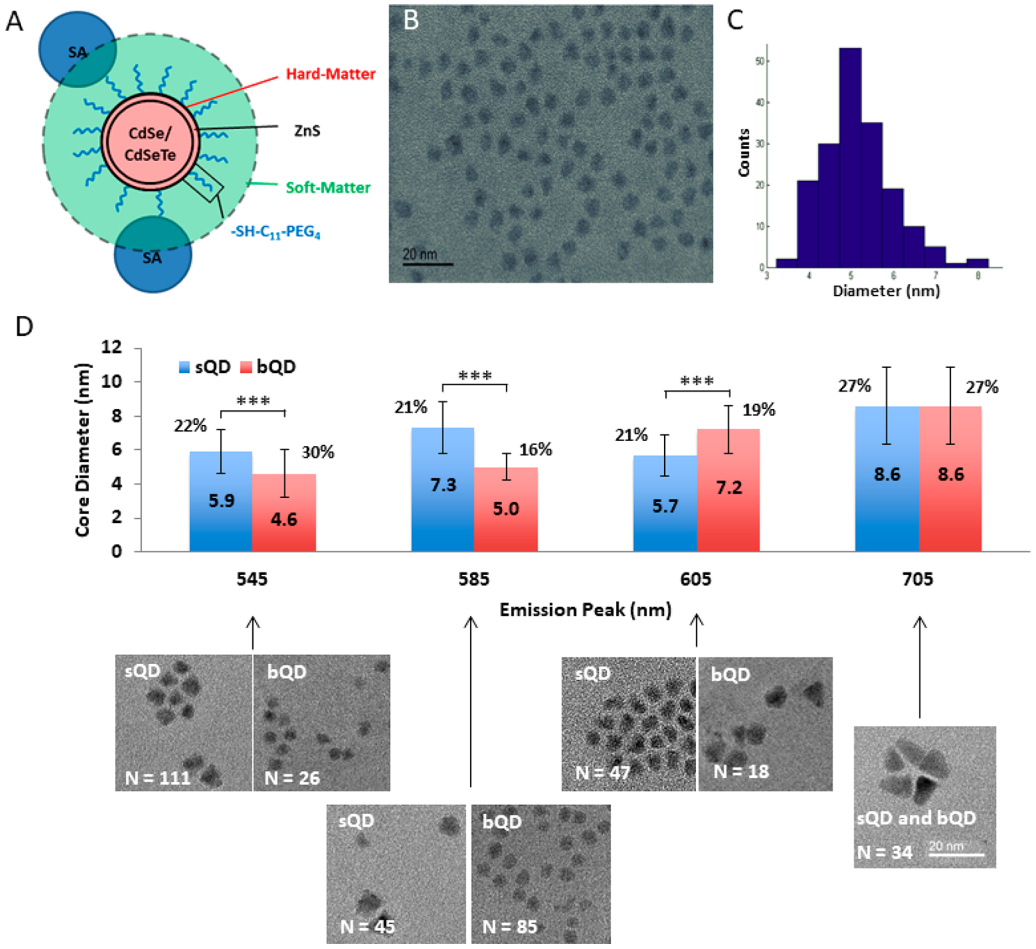

Figure 1. Overall structure and transmission electron microscopy analysis of QDs. (A) Schematic of the quantum dots comprising three distinct layers, the fluorescent core (CdSe-ZnS or CdSeTe-ZnS), the organic coating (HS-$(CH_2)_{11}$-$(OCH_2CH_2)_4$-OH), and streptavidin (SA). For commercial QDs the coating comprises both nonpolar ligands (e.g., oleic acid) and an amphiphilic polymer composed of poly(acrylic acid) modified with octylamine and polyethylene glycol. The red area indicates hard matter visible by TEM, and the green area indicates soft matter that can be measured by FCS. (B) Example TEM micrograph of a 585 nm bQD sample showing the core, with scale-bar indicating 20 nm. (C) Histogram of core diameters corresponding to this data set. Asterisks denote $p < 0.0001$ in all cases by one-tailed t test. (D) Average core diameter for QDs emitting at the same wavelengths, from two commercial suppliers, with error bars indicating standard deviation. Values next to error bars are relative standard deviation. Representative TEM micrograph of QDs are shown under each bar. All micrographs share the same error bar. More TEM micrographs are included in the Supporting Information.

groups (parts 2 and 3) present the greatest opportunity for decreasing hydrodynamic size while avoiding large trade-offs in function.[13] The reason is that commercial QDs are formulated for reliability and chemical stability, rather than minimized size, with a thick amphiphilic polymer coating and an excess of biofunctional groups like streptavidin that can bind with high affinity to biotin-conjugated targets. In contrast, we custom-designed QDs specifically to reduce the size over a range where neuronal synaptic receptor labeling is accurate, using thin hydrophilic layers of HS-$(CH_2)_{11}$-$(OCH_2CH_2)_4$-OH (11-mercaptoundecanoic acid tetraethylene glycol; MUTEG) as a coating. We further used a minimum number of streptavidin proteins as conjugation probes. This manuscript seeks to address the absolute contributions of each structure component to the total hydrodynamic diameter toward design rules to generate multiple QD colors with synaptic access.

QDs in this small size range present a technical challenge for accurate hydrodynamic size analysis. The highest resolution technique, size exclusion chromatography (SEC), compares the elution time from a column of microporous beads against that of a known size standard.[13−15] Unfortunately, the technique is simultaneously a purification method and strips the MUTEG ligands off of QDs, preventing elution. Another technique, dynamic light scattering (DLS), allows measurement based on the scattering of light by a particle. However, it is low resolution and best suited for nonabsorbing particles with large sizes (micron-scale), whereas nanometer-scale QDs exhibit small scattering cross sections and large absorption cross sections.[16,17] Fluorescence correlation spectroscopy (FCS)[18] relies on fluorescence instead of scattering and is well suited for size measurements of QDs due to their exceptional fluorescence intensities. However, blinking, optical saturation, and size heterogeneity require particular attention to accurately measure sizes with subnanometer resolution.[19−22] In this study, we use FCS to determine the hydrodynamic size contribution of QDs from coating layers (hydrophilic shell and streptavidin) and use transmission electron microscopy (TEM) to evaluate the inorganic cores.[23] Quantum dots at four distinct emission bands representing the most popular colors (545, 585, 605, and 705 nm) are tested. At each band the closest matching quantum dot core available from NN-

DOI: 10.1021/acs.jpcc.8b02516
J. Phys. Chem. C 2018, 122, 17406−17412

Labs (540, 560, 620) or from Invitrogen (705 nm) is used to produce the analogous sQD.

METHODS

FCS Instrument and Controls. Standard FCS systems rely on cross-correlation of signals from two avalanche photodiodes to eliminate uncorrelated electronic noise. Such electronic noise occurs in the ten to hundred nanosecond time scale, whereas diffusion dynamics of nanometer-sized particles such as quantum dots occur at the microsecond time scales. We therefore eliminated the second APD in our minimal FCS system to lower both cost and complexity (Figure 4). To test the system, published hydrodynamic size measurements from two different groups were reproduced. For a commercially available quantum dot (Invitrogen QD605 ITK) reported at 15.8 ± 0.6 nm diameter by FCS[26] and 15.0 nm diameter by HPLC from the manufacturer, we measured 15.5 ± 0.6 nm by our FCS, in excellent agreement. A laboratory-made polymer-coated quantum dot reported at 11.6 nm diameter by gel permeation chromatography[14] measured to 11.1 ± 0.7 nm by our FCS, again, in excellent agreement.

Theoretical Background on FCS. Here we provide a brief explanation of the theory of FCS. In order to determine the hydrodynamic diameter via FCS, a focal volume is formed by tightly focusing an excitation laser beam to the diffraction limit, through which fluorescent particles of interest can freely diffuse and be excited into emission. (More discussions of the subject, at greater length and depth, are readily available in refs 27−30.) The autocorrelation function $G(\tau)$ of the collected fluorescent signal $F(t)$ as a function of time delay, τ, is defined as

$$G(\tau) = \frac{\delta F(t)\cdot\delta F(t+\tau)}{\langle F(t)^2\rangle} \tag{1}$$

where $\delta F(t)$ indicates deviation of F at time t from the mean value and square brackets indicate time average. It is a monotonically decreasing function in τ with drops at any time constants inherent in the signal, one of which corresponds to the average time, τ_D, required for a particle to diffuse across the excitation focal volume. Assuming the focal volume to take the shape of a three-dimensional Gaussian, $G(\tau)$ is well fit by the expression

$$G(\tau) = \frac{1}{\langle N\rangle}\cdot\frac{1}{1+\frac{\tau}{\tau_D}}\cdot\frac{1}{\sqrt{1+\left(\frac{r_0}{z_0}\right)^2\cdot\frac{\tau}{\tau_D}}} \tag{2}$$

where $\langle N\rangle$ denotes the average number of particles in focal volume and r_0 and z_0 describe the lateral and axial width of the focal volume, respectively. r_0 and z_0 must be determined by the exact optics and calibrated for each system Supporting Information The diffusion coefficient D can be determined from the diffusion time constant τ_D by

$$\tau_D = \frac{{r_0}^2}{4D} \tag{3}$$

from which the Stokes−Einstein equation is then used to derive the hydrodynamic radius r_h assuming the particle is a sphere:

$$D = \frac{k_B T}{6\pi\eta r_h} \tag{4}$$

Organic dyes for which diffusion coefficients are well determined by other techniques such as NMR[28] are used for calibration. Due to the presence of triplet state, $G(\tau)$ must be fit with an extra term containing τ_T, the time constant of the dark or triplet state:[30]

$$G(\tau) = (1 - T + T\cdot e^{\tau/\tau_T})\cdot\frac{1}{\langle N\rangle}\cdot\frac{1}{1+\frac{\tau}{\tau_D}}\cdot\frac{1}{\sqrt{1+\left(\frac{r_0}{z_0}\right)^2\cdot\frac{\tau}{\tau_D}}} \tag{5}$$

In a well-aligned system, angstrom-level size resolution can be achieved.[17] The FCS system used in this study was custom-built, with fitting to these functions done with MATLAB scripts.

Quantum Dot Sources and Coatings. Organic CdSe/ZnS core/shells were purchased from NN-Labs with emission wavelengths of 540, 580, and 620 nm. CdSeTe/ZnS quantum dots with emission wavelength of 705 was purchased from Thermo Fisher Scientific. The manufacturer and catalog number for each batch are listed in Supplementary Table 1. To coat sQD, cores were encapsulated with 2.5% hydroxyl, 97.5% carboxyl terminus HS-$(CH_2)_{11}$-$(OCH_2\ CH_2)_4$-COOH. These sQD were then either characterized for hydrodynamic size as carboxyl QDs or further conjugated to SA prior to characterization. Coating and functionalization protocols were previously described.[10]

TEM Measurements. Commercial nonfunctionalized bQD were diluted in 10 mM borate buffer to a concentration of 10 nM for imaging. QD cores used for synthesis of sQD were diluted in hexane to a concentration of 10 nM for imaging. TEM samples were prepared by loading a drop of QD solution on an ultrathin carbon film TEM grid; then after a short moment (several minutes for QDs in buffer or several seconds for QDs in hexane), excess liquid was wicked off with a tissue. TEM images were acquired using a JEOL 2010 LaB_6 high-resolution transmission electron microscope at Frederick Seitz Materials Research Laboratory Central Research Facility at UIUC.

FCS Experiments. All measurements were performed on a home-built system based on a IX-71 frame (Olympus Ltd.) with the f = +180 mm tube lens removed. A single-mode pigtailed diode laser emitting at 488 nm (Coherent OBIS 488) aligned through a 60x/1.20 water immersion microscope objective (UPlanSApo, Olympus) served as the excitation source. The excitation wavelength was blocked from the emission path by a long-pass filter with cutoff 500 nm (Semrock). An external f = +150 mm lens focused the signal into a 50 μm core single mode fiber, which was then collected by a single photon counting module (SPCM-AQRH-14-FC). Autocorrelations were computed using an A320 FastFLIM system (ISS) with each data trace of 100 s correlated as ten sections of 10 s length, to check for self-consistency. Large spikes (>3σ) in the raw intensity trace and misshapen correlation curves are taken as indications for the presence of aggregates, and those data were discarded. The filtered autocorrelation curves were then fit using a MATLAB script.

RESULTS AND DISCUSSION

The contributions of core size, coating thickness, and streptavidin (SA) to the total hydrodynamic size are schematically depicted in Figure 1A for small quantum dots (sQD), which we designate as those coated with MUTEG, and

DOI: 10.1021/acs.jpcc.8b02516
J. Phys. Chem. C 2018, 122, 17406−17412

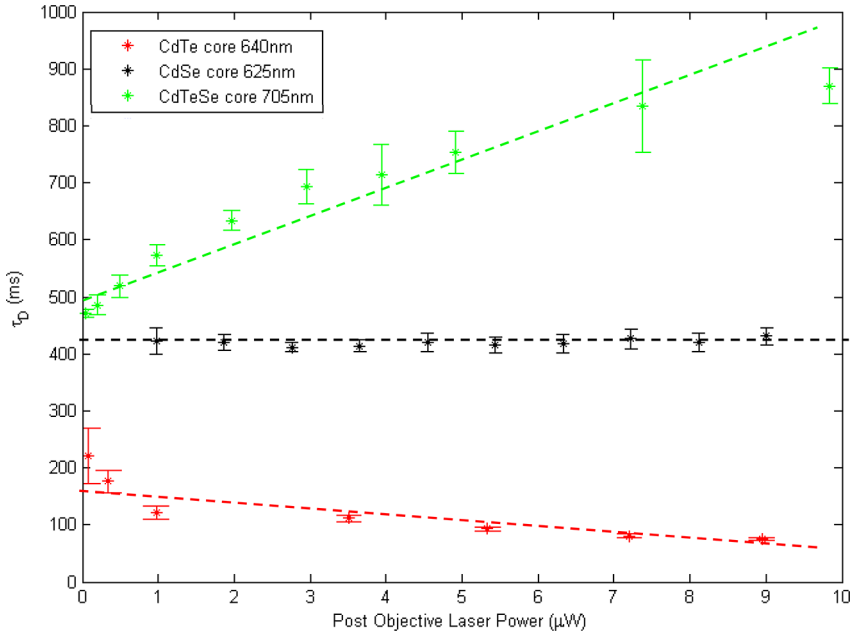

Figure 2. Plot of measured diffusion time constant τ_D as a function of excitation laser power post objective for three different quantum dots, CdTe core 640 nm (red), CdSe core 625 nm (black), and CdSeTe core 705 nm (green). Dotted lines are guides to indicate the distinct trends.

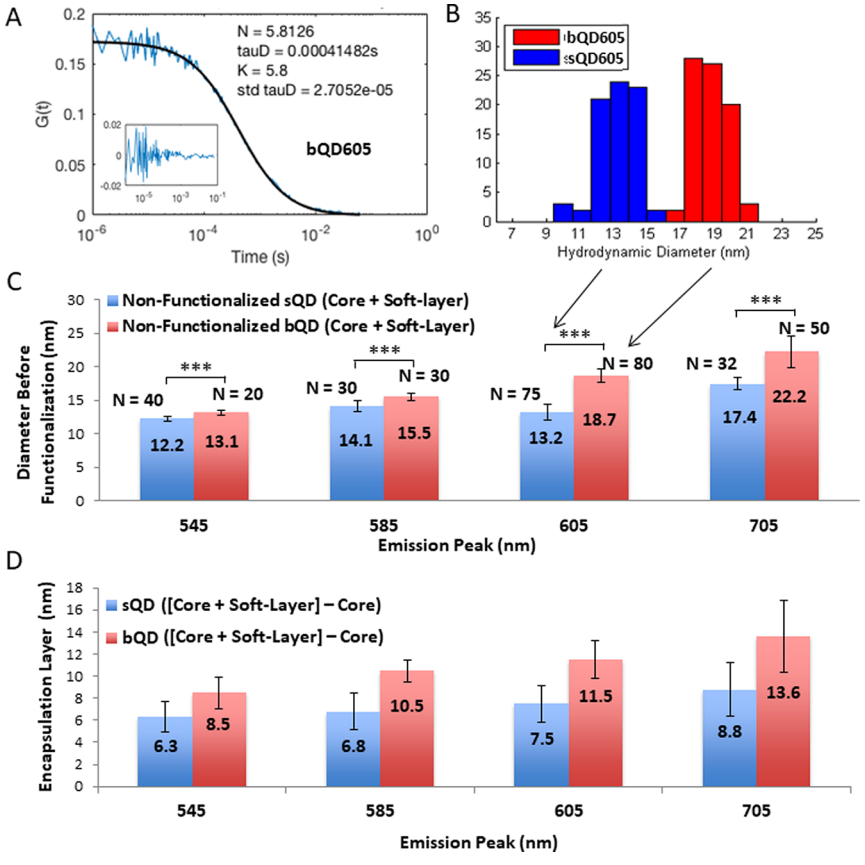

Figure 3. FCS of nonconjugated QDs. (A) Representative FCS autocorrelation function and fit. The inset shows the residual of the fit. (B) Histogram of measured hydrodynamic diameters for coated sQDs and bQDs with 605 nm emission. (C) Mean and standard deviation of hydrodynamic diameter for all QDs studied. (D) Mean contribution of encapsulation layer to final hydrodynamic diameter derived from subtracting corresponding TEM measurement.

commercial big quantum dots (bQD), which we designate as those coated with the standard commercial amphiphilic polymer. Three measurements were performed. First, TEM allowed determination of the crystalline core dimensions (hard-matter only). Second, FCS measurements on the same QD after coating with MUTEG provides the hydrodynamic

DOI: 10.1021/acs.jpcc.8b02516
J. Phys. Chem. C 2018, 122, 17406−17412

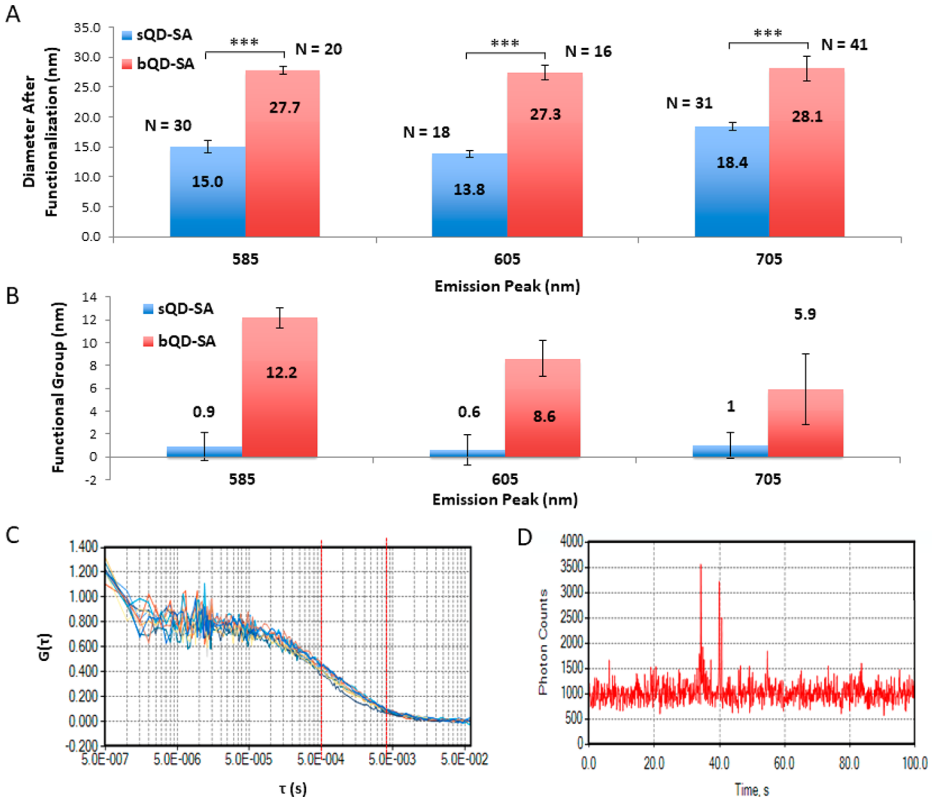

Figure 4. FCS on functionalized QDs. (A) Hydrodynamic diameter for streptavidin functionalized quantum dots. (B) Mean functional group contribution to hydrodynamic diameter derived from subtraction of corresponding nonfunctionalized quantum dot diameter. Only positive direction error bars shown. (C) Autocorrelation functions of ten consecutive 10 s traces, showing variation at around 10^{-4} to 10^{-3} s time scale. (D) Example fluorescent intensity trace during an FCS measurement, showing the presence of high-intensity aggregates in the commercial bQDs.

diameter, and the independent contribution of the coating after subtracting the TEM diameter. Third, FCS on the same QD after attachment to SA provides the contribution of SA by subtraction of the original FCS diameter. QDs with four different emission peak wavelengths (545, 585, 605, 705 nm) were tested, spanning the range of colors most commonly used. Cores for sQDs were purchased from NN-Labs for emission wavelengths 545, 585, and 605 nm, and from (potentially significantly different) Thermo Fisher Scientific for 705 nm emission. The complete sQDs were produced by our laboratory.[10] All four bQD were purchased from Thermo Fisher Scientific as amphiphilic polymer-coated QDs with and without SA.

Figure 1B–D shows TEM micrographs and size distributions for the QD cores used in this work. Each micrograph (Figure 1B) was imported into MATLAB for automated particle identification and measurement (see Supplementary Figure 1) to derive the average and standard deviation (SD) in core diameter. Figure 1C is a histogram of the data shown in Figure 1D, for the bQD-585 nm, and representative TEM images are shown in Figure 1D. Average diameters spanned between 4.6 and 8.6 nm depending on manufacturer and color, and relative SD varied between 16% and 30%. We note that the relative SD, for example the 27% value for 705 nm QDs, does not fully represent the three-dimensional heterogeneous structure of the QDs, for which heterogeneous polyhedral shapes were clear by TEM. Interestingly, QDs with the same emission wavelengths from different manufacturers (NN-Labs or Thermo Fisher) had substantially dissimilar ($p < 0.005$ by unpaired student's t test) sizes, likely due to differences in core and shell contributions to the nanocrystal.

To achieve reliable hydrodynamic size measurements with FCS, it is important to control for excitation intensity dependencies due to blinking[20,21] and saturation of the excited state.[19] Blinking events violate the central FCS assumption that a particle stops fluorescing only when it exits the illumination focal volume. Saturation effectively distorts the excitation profile from the assumed Gaussian shape. Both blinking and saturation are material-dependent effects that depend on core nanocrystal structure, size, and composition. The QDs used in this study with emission peaks at 545, 585, and 605 nm have CdSe cores, and at 705 nm, have CdSeTe cores, all of which contain an epitaxial wide bandgap shell composed of CdS and ZnS. To quantify the laser power dependence of FCS size measurements on these core characteristics, we measured the diffusion time constant for representative CdSe/ZnS and CdSeTe/ZnS QDs as a function of excitation intensity (Figure 2). The CdSe/ZnS QDs exhibited no variation in measured τ_D (proportional to size) over 2 orders of magnitude of laser power (0.1–10 μW). This implies minimal excited-state saturation. In stark contrast, we observed a dramatic increase in measured diffusion time constant with laser power for the CdSeTe core, implying excitation saturation. This is likely due to its substantially longer excited-state lifetime arising from its type-II electronic band structure. We also compared our results with a core-only CdTe QD reported by De Thomaz et al.,[21] which exhibited a major decrease in measured diffusion time constant with laser power for the CdTe core, consistent with the previous report, likely arising from the photochemical

DOI: 10.1021/acs.jpcc.8b02516
J. Phys. Chem. C 2018, 122, 17406–17412

lability of the CdTe material. Informed by these findings, we limit our laser power to 1 μW post objective for CdSe-core QDs and to 0.3 μW post objective for CdSeTe-core QDs. This will limit size errors to <5%.

FCS measurements on the aqueous coated QDs are shown in Figure 3. Panel A shows a representative example of an autocorrelation curve, and panel B shows histograms of measured hydrodynamic diameters for sQD and bQD with 605 nm emission wavelength. Measurements for the full set of QDs are in panel C. This shows the sQDs coated with MUTEG are consistently smaller than bQDs coated with the amphiphilic polymer, for the same cores. With increasing core size, the difference in hydrodynamic diameters (core + soft-layer) between sQD and bQD of the same emission peak generally increased, from 0.9 to 5.5 nm.

Figure 3D shows the coating thickness, calculated by subtracting the TEM-measured core diameter (Figure 1B) from the total FCS-measured diameter (Figure 3C). For the sQDs, the ligand layer increases from 6.3 nm (585 nm emission) to 8.8 nm (705 nm emission), indicating a monolayer thickness of ~3.2−4.4 nm, consistent with the fully extended length of MUTEG (~3.2 nm). The larger measured size for the largest cores likely derives from the different conformations of the tetraethylene glycol moiety on the surface as the surface becomes flatter, requiring a more extended, rather than coiled, polymer chain. Standard deviations propagated from those of the FCS and TEM measurements ($\sigma_{\text{encapsulation}} = \sqrt{\sigma_{\text{TEM}}^{\,2} + \sigma_{\text{FCS}}^{\,2}}$) are indicated as error bars for each encapsulation layer thickness.

Next, we performed FCS measurements on streptavidin-functionalized quantum dots, sQD-SA and bQD-SA (Figure 4). The sQD-SA were sQD functionalized with a minimum quantity of SA to yield probes that bind specifically to biotin in surface assays.[10] The SA-conjugated big quantum-dots, bQD-SA, were purchased as streptavidin conjugates from ThermoFisher Scientific. Hydrodynamic diameters for six SA conjugates are displayed in Figure 4A. Measurements are not shown for 545 nm sQD-SA conjugates because results were inconclusive, likely due to their very dim emission and tendency to aggregate, thereby increasing their size variation. Hydrodynamic diameters ranged from 13.8−18.4 nm for sQD-SA, and 27.3−28.1 nm for bQD-SA. Subtracting the measured diameter of nonfunctionalized QDs yielded the hydrodynamic contribution from the SA's. For the sQDs, SA contributed 0.9, 0.6, and 1.0 nm diameter versus 12.2, 9.6, and 5.9 nm for the bQDs (Figure 4B). The hydrodynamic diameter of SA (55kD mass) alone is approximately 5 nm,[24] and the diameter increase of the sQD-SA over nonfunctionalized sQD is consistent with 1−2 SA proteins per sQD-SA. The diameter increases for the bQD is clearly much larger due to the much larger number of SA per QD, described previously to be in the range 16−21 nm.[25] Some degree of aggregation for the commercial products may also have contributed; aggregation tends to appear between 10^{-4} and 10^{-3} s (Figure 4C) and can be seen in the variability of the FCS autocorrelation curves. (Each curve is a 10 s trace of a 100 s run.) As can be seen in Figure 4D, which is the fluorescence detection by the avalanche photodiode, this is likely because of occasional large and bright aggregates. Labeling of neuronal receptors using the ~18 nm diameter 705 nm sQD led to 20−30% more extra-synaptic labeling than smaller sQD. This suggests that the difference between ~12 nm diameter and ~18 nm diameter sQD-SA is enough to affect access to the narrow synaptic cleft, as we have seen (Figure S5).

CONCLUSION

By supplementing hydrodynamic diameters measured by FCS, with TEM-derived average CdSe/ZnS and CdSeTe/ZnS core diameters, we have demonstrated that encapsulating quantum dots with ligand layer HS-$(CH_2)_{11}$-$(OCH_2CH_2)_4$-OH leads to a particle for which the shell contributes 6.3−8.8 nm to the hydrodynamic diameter. Functionalizing the quantum dot with 1 to 2 SA per quantum dot leads to an increase in hydrodynamic diameter of only 0.6−1.0 nm, compared with an increase of 5.9−12.2 nm for commercial quantum dots. This decrease in diameter for the laboratory-made quantum dots is attributable to two primary factors: minimal number of functional groups and decreased coating thickness per quantum dot. Taking these factors into account means that a sQD has a diameter of ~14 nm, whereas a bQD has a diameter of ~18 nm. These attributes of our laboratory-made sQDs make these the superior choice for labeling of neuronal synapses where the cleft is physically constrained, as well as other *in vivo* situations with similar characteristics.

ASSOCIATED CONTENT

Supporting Information

The Supporting Information is available free of charge on the ACS Publications website at DOI: 10.1021/acs.jpcc.8b02516.

S1, Manufacturer and part number for all quantum dots and dyes used, as well as all diameter measurements; S2, schematic of the custom FCS system and table of all major components; S3, representative image processing algorithm output from MATLAB script for analysis of electron micrographs; S4, representative uncropped electron micrographs of quantum dot cores; S5, diffusion coefficients of neuronal receptor AMPAR labeled by 705 and 615 nm; S6, histogram of measured hydrodynamic diameters of quantum dots at emission 585 nm; S7, histogram of measured hydrodynamic diameters of quantum dots at emission 605 nm; S8, histogram of measured hydrodynamic diameters of quantum dots at emission 705 nm; S9, gel electrophoresis of sQD and sQD-SAl coating and streptavidin conjugation protocol for small quantum dots (sQD and sQD-SA) (PDF)

AUTHOR INFORMATION

Corresponding Author

*P. R. Selvin. E-mail: selvin@illinois.edu.

ORCID

Janet Y. Sheung: 0000-0003-4694-9740

Notes

The authors declare no competing financial interest.

ACKNOWLEDGMENTS

We are grateful to ISS Inc. for their loan of equipment and software for our FCS system. We are grateful to Duncan Nall for help in the initial stages of instrument building. J.S. is grateful to Pauline Maffre and Bob Hasson for informative discussions. J.S. acknowledges her fellowship support from Inprentus (through NSF SBIR grant). This work was partially

DOI: 10.1021/acs.jpcc.8b02516
J. Phys. Chem. C 2018, 122, 17406−17412

supported by NIH GM108578 and NS100019 and NSF PHY 1430124 (to PRS).

REFERENCES

(1) Alivisatos, A. P. Semiconductor Clusters, Nanocrystals, and Quantum Dots. *Science* **1996**, *271*, 933−937.
(2) Bawendi, M. G.; Steigerwald, M. L.; Brus, L. E. The Quantum Mechanics Of Larger Semiconductor Clusters. *Annu. Rev. Phys. Chem.* **1990**, *41*, 477−496.
(3) Gerion, D.; Pinaud, F.; Williams, S. C.; Parak, W. J.; Zanchet, D.; Weiss, S.; Alivisatos, A. P. Synthesis and Properties of Biocompatible Water-Soluble Silica-Coated CdSe/ZnS Semiconductor Quantum Dots. *J. Phys. Chem. B* **2001**, *105*, 8861−8871.
(4) Rao, J.; Dragulescu-Andrasi, A.; Yao, H. Fluorescence Imaging *in vivo*: Recent Advances. *Curr. Opin. Biotechnol.* **2007**, *18*, 17−25.
(5) Teng, K. W.; Ishitsuka, Y.; Ren, P.; Youn, Y.; Deng, X.; Ge, P.; Lee, S. H.; Belmont, A. S.; Selvin, P. R. Labeling proteins inside living cells using external fluorophores for microscopy. *eLife* **2016**, *5*, e20378.
(6) Hoffman, M. T.; Sheung, J. Y.; Selvin, P. R. Fluorescence imaging with one nanometer accuracy: *in vitro* and *in vivo* studies of molecular motors. *Methods Mol. Biol.* **2011**, *778*, 33−56.
(7) Qdot Nanocrystals Technology Overview. Retrieved from https://www.thermofisher.com/us/en/home/brands/molecular-probes/key-molecular-probes-products/qdot/technology-overview.html#bioconjugate.
(8) Groc, L.; Lafourcade, M.; Heine, M.; Renner, M.; Racine, V.; Sibarita, J.-B.; Lounis, B.; Choquet, D.; Cognet, L. Surface trafficking of neurotransmitter receptor: comparison between single-molecule/quantum dot strategies. *J. Neurosci.* **2007**, *27*, 12433−12437.
(9) Opazo, P.; Labrecque, S.; Tigaret, C. M.; Frouin, A.; Wiseman, P. W.; De Koninck, P.; Choquet, D. CaMKII Triggers the Diffusional Trapping of Surface AMPARs through Phosphorylation of Stargazin. *Neuron* **2010**, *67*, 239−252.
(10) Cai, E.; Ge, P.; Lee, S. H.; Jeyifous, O.; Wang, Y.; Liu, Y.; Wilson, K. M.; Lim, S. J.; Baird, M. A.; Stone, J. E.; et al. Stable small quantum dots for synaptic receptor tracking on live neurons. *Angew. Chem., Int. Ed.* **2014**, *53*, 12484−12488.
(11) Lee, S. H.; Jin, C.; Cai, E.; Ge, P.; Ishitsuka, Y.; Teng, K. W.; de Thomaz, A. A.; Nall, D. L.; Baday, M.; Jeyifous, O. Super-resolution Imaging of Synaptic and Extra-synaptic Pools of AMPA Receptors with Different- sized Fluorescent Probes. *eLife* **2017**, *6*, e27744.
(12) Algar, W. R.; Tavares, A. J.; Krull, U. J. Beyond labels: A review of the application of quantum dots as integrated components of assays, bioprobes, and biosensors utilizing optical transduction. *Anal. Chim. Acta* **2010**, *673*, 1−25.
(13) Smith, A. M.; Duan, H.; Rhyner, M. N.; Ruan, G.; Nie, S. A systematic examination of surface coatings on the optical and chemical properties of semiconductor quantum dots. *Phys. Chem. Chem. Phys.* **2006**, *8*, 3895−3903.
(14) Ma, L.; Tu, C.; Le, P.; Chitoor, S.; Lim, S. J.; Zahid, M. U.; Teng, K. W.; Ge, P.; Selvin, P. R.; Smith, A. M. Multidentate Polymer Coatings for Compact and Homogeneous Quantum Dots with Efficient Bioconjugation. *J. Am. Chem. Soc.* **2016**, *138*, 3382−3394.
(15) Parris, N. A. *Instrumental liquid chromatography: a practical manual on high-performance liquid chromatographic methods*; Elsevier, 2000; p 27.
(16) Choi, H. S.; Liu, W.; Misra, P.; Tanaka, E.; Zimmer, J. P.; Itty Ipe, B.; Bawendi, M. G.; Frangioni, J. V. Renal clearance of quantum dots. *Nat. Biotechnol.* **2007**, *25*, 1165−1170.
(17) Goldburg, W. I. Dynamic light scattering. *Am. J. Phys.* **1999**, *67*, 1152.
(18) Schwille, P. Fluorescence correlation spectroscopy and its potential for intracellular applications. *Cell Biochem. Biophys.* **2001**, *34*, 383−408.
(19) Nienhaus, G. U.; Maffre, P.; Nienhaus, K. Studying the protein corona on nanoparticles by FCS. *Methods Enzymol.* **2013**, *519*, 115−137.
(20) Doose, S.; Tsay, J. M.; Pinaud, F.; Weiss, S. Comparison of photophysical and colloidal properties of biocompatible semiconductor nanocrystals using fluorescence correlation spectroscopy. *Anal. Chem.* **2005**, *77*, 2235−2242.
(21) De Thomaz, A. A.; Almeida, D. B.; Pelegati, V. B.; Carvalho, H. F.; Cesar, C. L. Measurement of the hydrodynamic radius of quantum dots by fluorescence correlation spectroscopy excluding blinking. *J. Phys. Chem. B* **2015**, *119*, 4294−4299.
(22) Liedl, T.; Keller, S.; Simmel, F. C.; Rädler, J. O.; Parak, W. J. Fluorescent nanocrystals as colloidal probes in complex fluids measured by fluorescence correlation spectroscopy. *Small* **2005**, *1*, 997−1003.
(23) Williams, D. B.; Carter, C. B. *The transmission electron microscope*; Springer, 1996.
(24) Erickson, H. P. Size and shape of protein molecules at the nanometer level determined by sedimentation, gel filtration, and electron microscopy. *Biol. Proced. Online* **2009**, *11*, 32−51.
(25) Mittal, R.; Bruchez, M. P. Biotin-4-fluorescein based fluorescence quenching assay for determination of biotin binding capacity of streptavidin conjugated quantum dots. *Bioconjugate Chem.* **2011**, *22*, 362−368.
(26) Maffre, P.; Brandholt, S.; Nienhaus, K.; Shang, L.; Parak, W. J.; Nienhaus, G. U. Effects of surface functionalization on the adsorption of human serum albumin onto nanoparticles - a fluorescence correlation spectroscopy study. *Beilstein J. Nanotechnol.* **2014**, *5*, 2036−2047.
(27) Elson, E. L.; Magde, D. Fluorescence correlation spectroscopy. I. Conceptual basis and theory. *Biopolymers* **1974**, *13*, 1−27.
(28) Magde, D.; Elson, E. L.; Webb, W. W. Fluorescence Correlation Spectroscopy. II. An Experimental Realization. *Biopolymers* **1974**, *13*, 29−61.
(29) Rigler, R.; Mets, U.; Widengren, J.; Kask, P. Fluorescence Correlation Spectroscopy With High Count Rate and Low-Background - Analysis of Translational Diffusion. *Eur. Biophys. J.* **1993**, *22*, 169−175.
(30) Schwille, P.; Kummer, S.; Heikai, A. A.; Moerner, W. E.; Webb, W. W. Fluorescence correlation spectroscopy reveals fast optical excitation-driven intramolecular dynamics of yellow fluorescent proteins. *Proc. Natl. Acad. Sci. U. S. A.* **2000**, *97*, 151−156.

DOI: 10.1021/acs.jpcc.8b02516
J. Phys. Chem. C 2018, 122, 17406−17412